Leaf Geometric Characteristics of Monstera deliciosa: Effects on Tribological and Friction-induced Vibration Behaviors of Rolling Bearings under Starved Lubrication

Risheng Long [1,2,✉] – Jiaxin Chen[2] – Fangfeng Gao[2] – Ruidan Huang[2] – Shuzhi Gao[2] – Lin Zong[3,✉✉]

1 School of Mechanical Engineering, Shenyang Ligong University, China
2 Equipment Reliability Institute, Shenyang University of Chemical Technology, Shenyang, China
3 School of Mechanical and Power Engineering, Shenyang University of Chemical Technology, Shenyang, China

✉ etomi@163.com, ✉✉ zl40145173@163.com

Abstract *To prolong the service life of the rolling bearings and improve the reliability of the associated mechanical systems, inspired by the leaves of Monstera deliciosa, eleven biomimetic texture patterns, featuring various leaf-geometry characteristics – such as leaf-veins, elliptical holes, and their combinations – were designed and prepared on the raceway of the shaft washer of cylindrical rollers thrust bearings using a laser surface texturing method. The effects of these leaf-inspired patterns on the tribological and friction-induced vibration performance of rolling bearings were systematically investigated under starved lubrication conditions. The results show that a significant "superposition effect" on vibration signals was observed in the earlier stages of testing, but this effect diminished over time. Larger aspect ratios of elliptical holes did not improve the friction-wear performance of the biomimetic textured groups. When the elliptic area was larger, the bearing experienced relatively lower wear losses, higher average coefficients of friction, and greater fluctuations in time-domain vibration signals. The influence of different elliptic areas on the frequency-domain vibration signals was minimal. This work would provide a valuable insight into the raceway optimization of rolling bearings.*

Keywords *rolling bearings; biomimetic surface texture; tribological and friction-induced vibration; starved lubrication*

Highlights

- *Several biomimetic texture patterns were designed inspired by the leaf-geometry characteristics of Monstera deliciosa.*
- *These biomimetic texture patterns were introduced to the raceways of rolling bearings.*
- *The performances of biomimetic textured cylindrical roller thrust bearings were researched under starved lubrication conditions.*
- *The influence mechanism of biomimetic texture patterns on the tribological and vibration behavior of rolling bearings was discussed.*

1 INTRODUCTION

Friction and wear, which account for approximately one-fifth of global energy consumption, are unavoidable challenges in most mechanical systems [1,2]. These issues not only result in significant material and energy losses but also directly impact the efficiency of the contact interfaces, shorten the operational life-span of machinery, and pose substantial safety risks [3]. To reduce friction and wear in tribo-pairs, whether the rolling, sliding or rolling-sliding, various methods have been explored, such as surface texturing (ST) [3,4], self-lubricating coatings [5], hard coatings [6,7], manufacturing errors reducing [8] and innovative structures [9]. Among these, ST has garnered widespread attention worldwide due to its ability to enhance lubrication [10-12], trap wear debris [3,4,12], and generate hydrodynamic pressure effects [13,14]. In fact, ST has proven to be effective and has been applied in numerous industrial fields over the past decade [15-18].

Nature is an incredible teacher and has inspired countless innovative designs in the field of engineering. Over millions of years of evolution, the flora and fauna that have survived to this day have developed diverse structural forms, offering valuable insights into surface texturing design to address mechanical friction problems [3,19]. Inspired by various biological surfaces, Wang et al. [20] designed and prepared two types of multi-hierarchical textures (MHTs) on AISI 440C steel using femtosecond laser ablation and coating technology. These textures resulted in significant wear resistance under low loads and high frequencies. Liu et al. [21] mimicked the scales of loach to create a bionic textured surface through micro 3D metal printing technology, finding that it reduced friction and wear in sliding pairs under low-speed, high-load and starved lubrication conditions. Qin et al. [22] mimicked the unique morphology of the shark skin, combining air plasma treatment and soft lithography to study its effect on the stick-slip behavior of polydimethylsiloxane (PDMS). Li et al. [23] mimicked the structure of a tree frog's toe pad to study the effects of bionic and hexagonal surface textures on the application of magneto-fluidic vibration isolators (MFSAs), discovering that both textures enhanced the wear resistance of MFSAs. Wang et al. [24] used the surface of seashells as a model and conducted numerical simulations to study the effect of biomimetic multi-scale composite textures on the lubrication of axial piston pump friction pairs under seawater lubrication. They found that biomimetic surfaces improved load-bearing capacity and reduce the coefficient of friction (COF), with groove combination textures providing superior lubrication performance. Khatri et al. [25] mimicked the veins of linden leaves and optimized the performance of vein-bionic textured dynamic plain bearings using a genetic algorithm (GA). The results showed that the optimized vein-bionic textures significantly improved the static and dynamic performance of the bearings, reducing cavitation and friction. Zhang et al. [26] simulated the surface features of Gulf oyster shells and applied them to the tooth surfaces of gears. The results showed that the gears with bionic textures performed better in terms of lubrication efficiency,

heat dissipation, and reduction of mechanical efficiency loss. Song et al. [27] inspired by the microstructures of earthworms, carps, sharks, and beetles, prepared different biomimetic textures on the surface of YT15 alloy steel. They found that all types of textures improved friction-wear performance and enhanced fluid dynamic lubrication. Liang et al. [28] used computational fluid dynamics (CFD) simulation and tribo- experiments to study the performance of an axial piston pump slide shoe-pair with biomimetic composite textures (ball-pit-ball-ridge), mimicking the dung beetle, under seawater lubrication. They found that the textured slide shoe-pair improved total load capacity, reduced COF, and enhanced wear resistance.

Leaves play a crucial role in the life system of plants and have evolved various properties through natural selection to adapt to harsh environments [3]. Among the typical structures of leaves, veins are particularly important, as they contribute to the mechanical strength and help maintain low internal strain energy [29]. Long et al. [30] designed six types of vein-bionic textures based on the leaves of *Forsythia*, *Clausena lansiu*, *Ash*, *Purple leaf plum*, *Pipal* and *Apricot*, and investigated their effect on the tribological behavior of the cylindrical roller thrust bearings (CRTBs). Both *Monstera deliciosa* and *Monstera friedrichsthalii* are perennial, woody, climbing evergreen shrubs native to the rainforests of South America. Their oval-shaped leaves feature gaps and "cheese-like" holes, see Fig. 1. These leaf-geometry characteristics help prevent damage from adverse environmental conditions, such as strong winds and torrential rains, in their natural rainforest habitat [31,32]. Long et al. [33] replicated the distinctive "cheese-like" structures of the *Monstera friedrichsthalii* leaves using laser marking technology to investigate how the angle and symmetry of leaf-vein textures affect the tribological and friction-induced vibration behavior of CRTBs. They found that asymmetrical leaf-inspired textures, with a 45°angle between the main vein and the costal veins, significantly improved the tribological performance and reduced friction-induced vibration in the rolling bearings.

The friction-reducing and anti-wear properties of textured surfaces are significantly influenced by the characteristics of the texture [34], such a, shape (e.g., dimples [13,35,36], grooves [37], veins [3,30,33], scales [21]), area densities [36,37], and their combined effects [12,14,15]. Based on previous works [3,30], to fill the gap in the study of the biomimetic textures inspired by *Monstera friedrichsthalii* in [33], various biomimetic patterns were introduced to further systematically reveal the synergistic relationship between elliptical holes and leaf veins, as well as the influence of elliptical hole area on the friction and vibration performance of textured CRTBs were researched under starved lubrication. The remainder of this paper is organized as follows: In Section 2, the design and research methods of biomimetic textures were explained in detail; In Section 3, the experimental data were compared and analyzed from four aspects; In Section 4, the synergistic mechanism between leaf veins and elliptical holes, as well as the influence mechanism of elliptical hole area size on bearing friction and vibration performance, were discussed. The findings would provide valuable insights for optimizing the contact interface design of rolling bearings and other mechanical components.

2 MATERIALS AND METHODS

2.1 Design and Preparation

A typical 81107TN bearing (YFB, Changzhou, China) consists of a shaft washer (WS81107), 18-20 rollers [3,30], a black nylon cage (PA 66) and a housing washer (GS81107, see Fig. 2a). The main dimensions and materials of these components are summarized in Table 1.

Table 1. The dimensions, materials and quantities of the main components of 81107TN bearing

Component	Inner diameter [mm]	Outer diameter [mm]	Height [mm]	Material	Quantity
Shaft washer	35	52	3.5	GCr15	1
Housing washer	37	52	3.5	GCr15	1
Roller	-	5	5	GCr15	18
Cage	35	52	4	PA66	1

Inspired by the leaves of *Monstera deliciosa*, eleven leaf-geometry patterns, labeled as C01-C11 (see Figs. 1 and 2c), were designed and applied to the raceways of the shaft washers of 81107TN bearings. As shown in Table 2, patterns C03, C05, C07, C09, C11 are combinations of C02, C04, C06, C08, C10 with C01, respectively. A smooth group, labeled as C12, was also introduced [3,30]. Based on the results from [31], the costal veins and elliptic holes (60 sets) were asymmetrically distributed. The angle between the main vein and the costal veins was

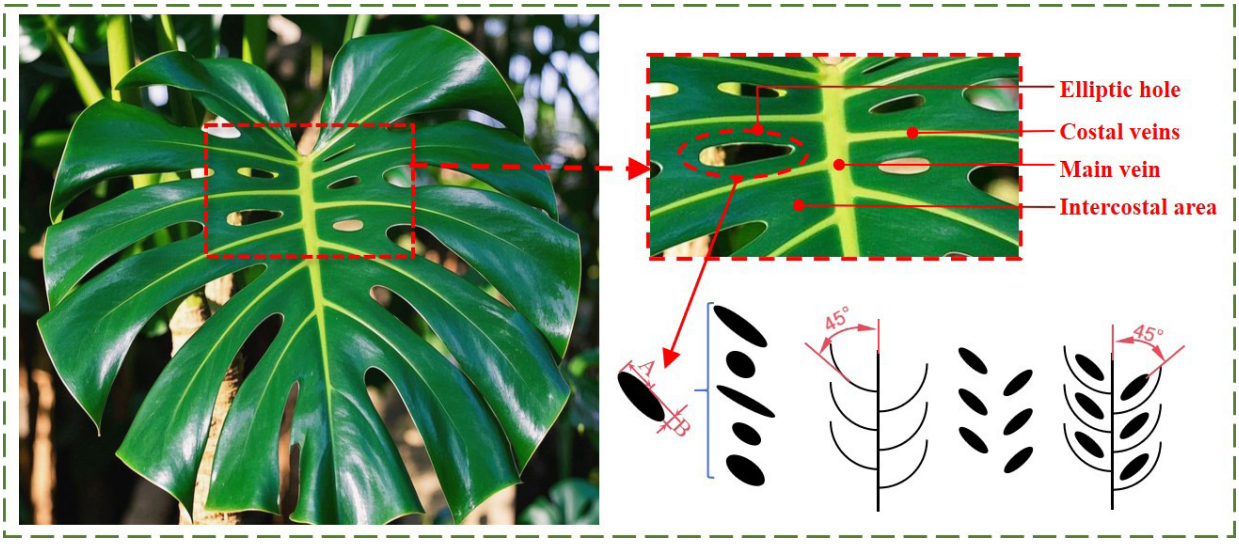

Fig. 1. Leaf of Monstera deliciosa and its main leaf-geometry characteristics

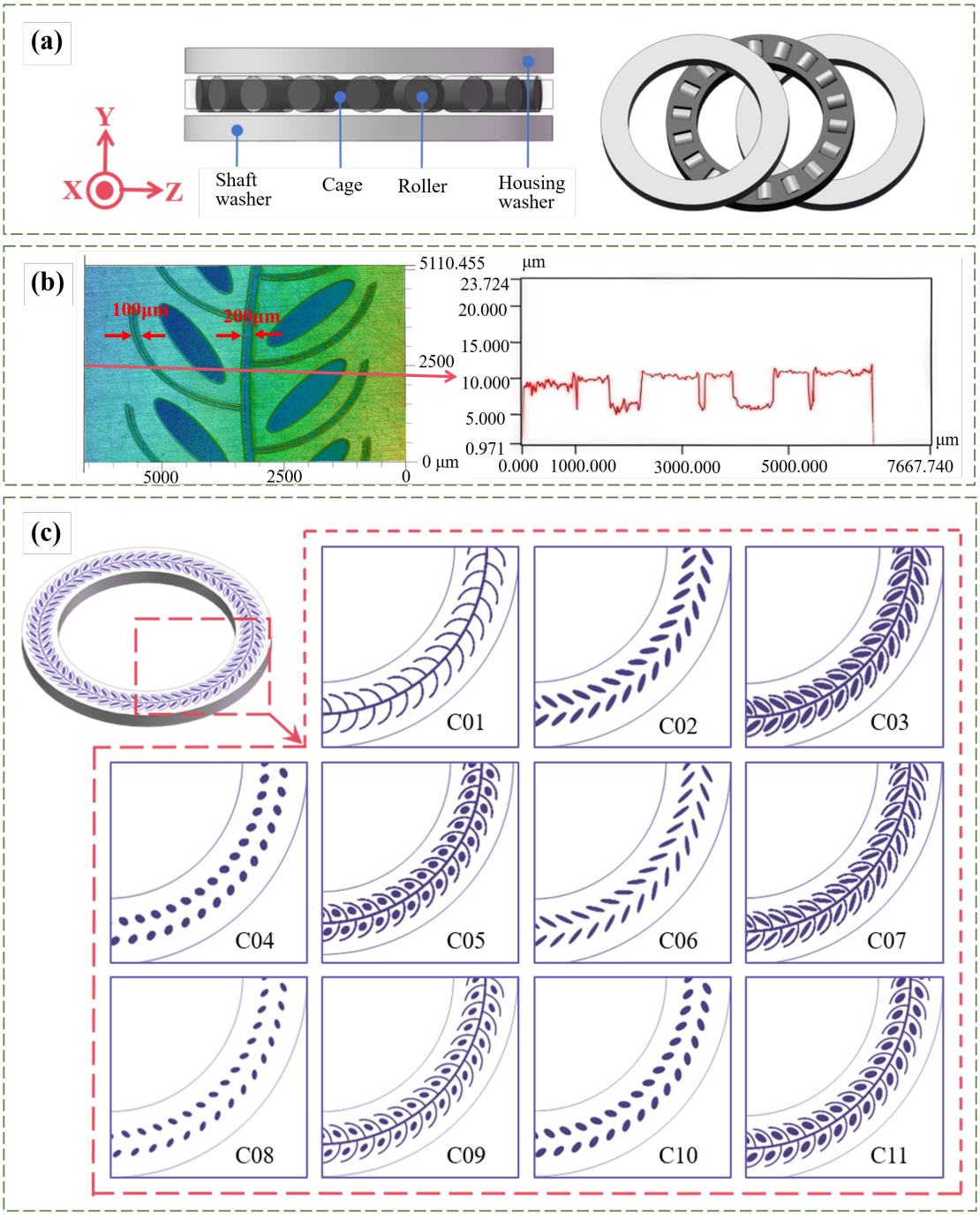

Fig. 2. Bearing model and the Monstera deliciosa inspired leaf-geometry patterns; a) 3D model of the 81107 bearing, b) 3D morphology and dimensions of the bionic textures, and c) sketch of the leaf-geometry patterns designed

set at 45°. The widths of the main veins and costal veins were 200 μm and 100 μm, respectively, with a depth of 5 μm, matching the depth of the elliptical holes (see Fig. 2b). The actual texture width and depth obtained were 200±2 μm, 100±1.2 μm, and 5±0.8 μm, respectively (see Table S1 in the Supplementary Material) [40].

To prepare the biomimetic textures on the raceways of the shaft washers, a laser marking machine (PL100-30W, Wanquan, Shenyang, China) was used with the following parameters: average maximum power of 12 W, laser spot diameter of 30 μm, pulse energy density of 2.8 J/cm², laser pulse frequency of 80 kHz, scanning speeds of 94 mm/s (for veins) and 85 mm/s (for elliptical holes). The patterns were marked in a single pass, and the prepared samples were then ultrasonic cleaned in ethanol for 15 minutes before the wear tests. The actual dimensions of the veins and holes can be found in the Supplementary Material.

2.2 Tribological Experiments

A vertical universal wear tester (MMW-1A, Huaxing, China) was used to investigate the tribological and friction-induced vibration performance of rolling bearings under starved lubrication conditions. To simulate the severe working conditions, only 4 mg of lubricant (HX7 SW-30, Shell, China) was applied to the raceway of the shaft washer before each test [3,30,33]. The photo of the wear tester and

Table 2. Test groups and their leaf-geometry parameters

Group	Costal vein	Elliptic hole	Semi-long axis A [μm]	Semi-short axis B [μm]	A/B ratio*	Elliptic area [mm^2]	Area ratio [%]
C01	√	–	–	–	–	–	10.76
C02	–	√	1200	300	4.0	0.36π	19.86
C03	√	√	1200	300	4.0	0.36π	30.62
C04	–	√	600	400	1.5	0.24π	13.24
C05	√	√	600	400	1.5	0.24π	24
C06	–	√	1200	200	6.0	0.24π	13.24
C07	√	√	1200	200	6.0	0.24π	24
C08	–	√	600	300	2.0	0.18π	9.93
C09	√	√	600	300	2.0	0.18π	20.69
C10	–	√	800	400	2.0	0.32π	17.65
C11	√	√	800	400	2.0	0.32π	28.41
C12	–	–	–	–	–	–	–

* A/B ratio: the ratio of the long-axis to the short-axis.

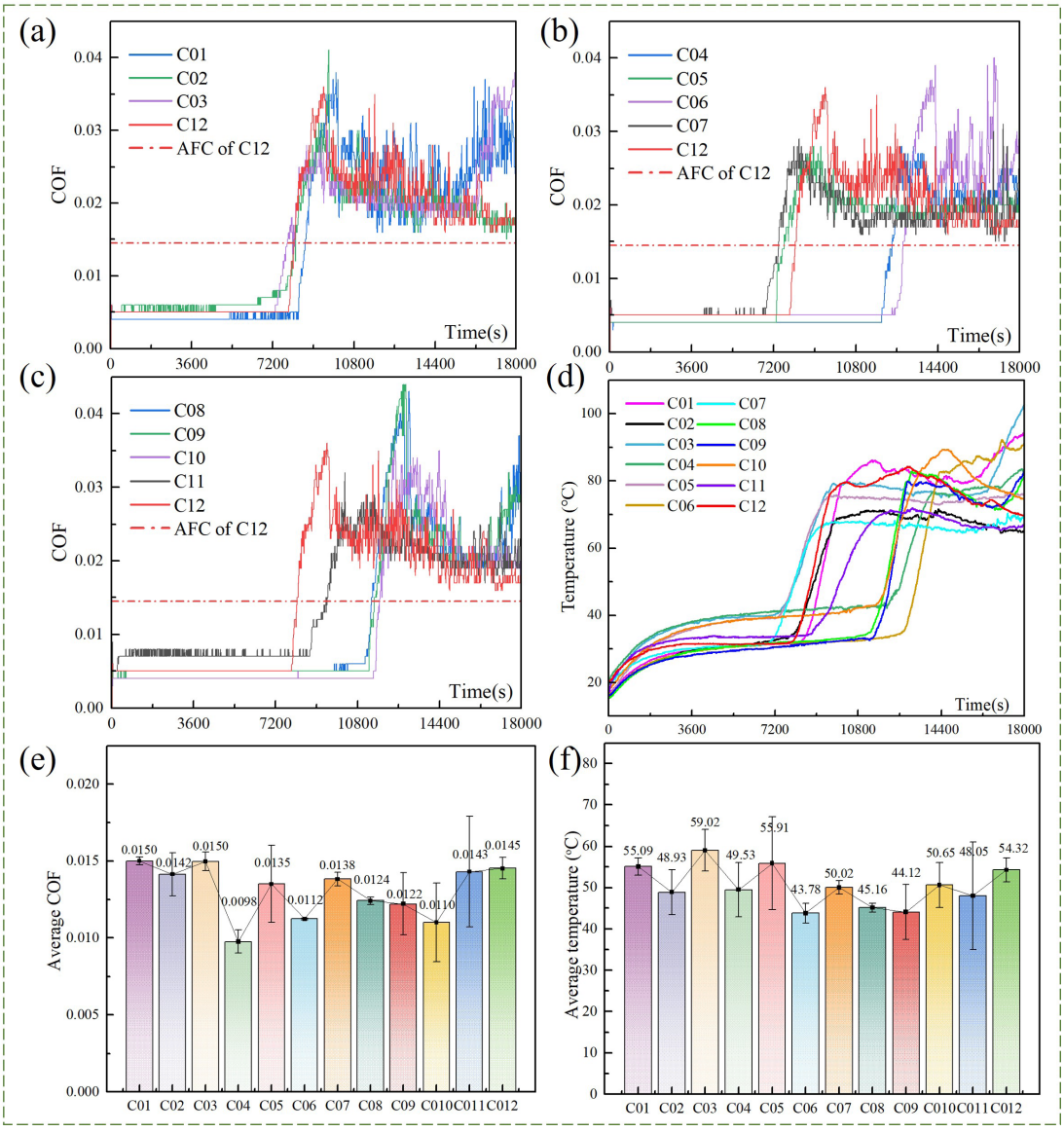

Fig. 3. Representative COF-time curves and other data (n=3) of different groups under starved lubrication; a) C01-C03, b) C04-C07, c) C08-C11, d) C01-C12, e) average COFs, and f) average temperatures

details of the lubricant parameters can be found in the Supplementary Material. The bearing was then mounted in a customized chucking and the whole process is also described in the Supplementary Material.

Each test was conducted under an axial load of 4600 N and a rotational speed of 250 rpm for duration of 5 hours. Each group was repeated three times (i.e., $n=3$), using three new bearings for each test to ensure repeatability, objectivity, and accuracy. In total, 36 sets of bearings were consumed in this work, including 33 biomimetic textured bearings and 3 smooth bearings.

A high-precision multi-channel data acquisition system (LMS SCM 2E02, Siemens, Germany) was employed to collect the vibration signals in the X-axis/tangential and Y-axis/normal directions (see Fig. 2a) during each test. The signals were recorded through an accelerometer fixed on the protruding platform of the lower chuck (see the Supplementary Material). The bearing was sampled every 30 min with a sampling frequency of 12.8 kHz. Each sampling was taken three times consecutively, with each recording lasting 30 s. After each test, a 3D surface profiler (VK-X1050, Keyence, Japan) and an electronic analytical balance (EX225D, Ohaus, 0.01 mg readability) were used to characterize the worn raceway and measure the wear amount.

3 EXPERIMENTAL RESULTS

3.1 Coefficient of Friction

Figure 3 shows the representative COF-time and temperature-time curves for different groups, along with their averages under oil-starved lubrication. Note that: The average for each group presents the average of the entire curve, whether for COF-time or temperature-time. As shown in the figure, each COF curve went through three distinctly different stages: the mild-friction stage (S1), followed by the rapid-rising stage (S2), and then the severe-fluctuating stage (S3) [33,35]. Notably, most of the leaf-geometry textured groups experienced significantly longer mild-friction stages and entered the second stage much later (see Figs. 3a-c), except for C03, C05, and C07, whose mild-friction durations were even slightly shorter than that of the smooth group. This can be attributed the fact that the biomimetic textures can store lubricant and can realize the "secondary lubrication" in the earlier stages, thereby extending the effective action-time of the lubricant film [3].

Due to the centrifugal force generated during the rapid rotation of the shaft washers [38], the lubricant was continuously consumed, either thrown out or deteriorated, and the bearings gradually entered the boundary lubrication, i.e., the second stage (S2). This transition led to a sharp increase in the COF-time and temperature-time curves [35]. Meanwhile, a significant amount of nylon debris was generated due to the direct contact between the rollers and the cage pockets, resulting in notable increases in the rotational resistance of the "washers-rollers-cage" systems [35-37]. As a result, the COF curves rose sharply and most of the wear on the components occurred during this stage. Furthermore, as shown in Fig. 3d, the rapid rise in each temperature-time curve corresponded closely with the fast-rising phase of the COF-time curve.

Under the combined action of the rollers and centrifugal force, as the nylon transfer film became more uniform and stable, the bearings' temperature also stabilized. At this point, the COF curves entered the third stage (S3) [33,37]. The running resistance of the bearings increased and fluctuated violently due to wear on the raceway and the relatively large COF of the nylon-steel tribo-interface [36,37]. Among all groups, the average COF of C04 was the lowest and just 0.0098.

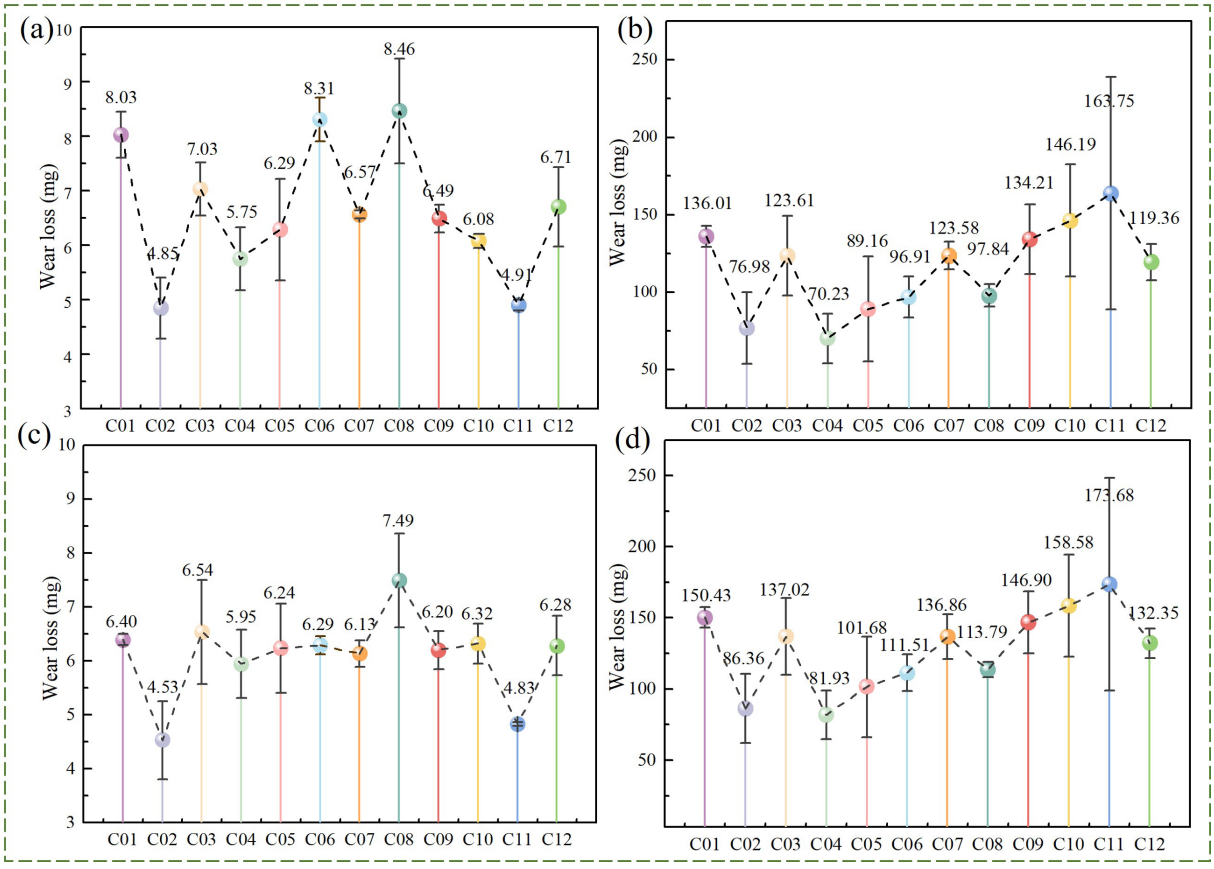

Fig. 4. Wear amounts (n=3) of the main components of different groups; a) shaft washers, b) cage-assembles, c) seat washers, and d) total wear losses of three main components

3.2 Wear Amounts and Worn Surfaces

Figure 4 shows the wear amounts of the main components (i.e., shaft washers, housing washers and cage-assembles) for different groups. As shown in the figure, the wear amounts of the cage assemblies followed a trend similar to that of the average COFs in Fig. 3e, differing from the trends observed for the two washers. This is because the leaf-geometry textures help trap debris, preventing it from contributing to three-body wear, and thus protect the raceways from severe wear [3,30,33]. Among all groups, the wear losses of the shaft washers for C02 and C11 were relatively small, at 4.85 mg and 4.91 mg, respectively, followed by the mass loss of the shaft washer for C04 (5.75 mg).

Figure 5 shows the worn surfaces of the shaft washers for different groups before and after ultrasonic cleaning. As shown in Fig. 5a, the transfer film left on the unwashed worn surfaces with elliptical holes only (i.e., C2, C4, C6, C8 and C10) was less than that on the surfaces with composite textures (i.e., C03, C05, C07, C09, and C11). After ultrasonic cleaning, it is evident that the high-temperature zones on the raceways of C01 and C12 were significantly larger than those of the other groups. Compared to C1, C2, C4, C6, C8, C10 and C12, the high-temperature ablation and wear marks on the worn surfaces of C03, C05, C07, C09 and C11 were much less severe. Therefore, it can be reasonably inferred that the elliptical-holes, when coupled with the leaf-veins, formed a synergistic mechanism that significantly enhanced the anti-wear performance in the middle regions of the raceways (see Fig. 5b). This mechanism improved the heat transfer in the "washers-rollers-cage" system and reduced the high-temperature marks on the worn surfaces [3,35]. Based on the worn surfaces, the failure mode of the rolling bearings in this work was primarily severe abrasive wear combined with localized fatigue pitting [3,30,33,35-37]. More images can be found in the Supplementary Material. Due to the relatively small values, the impact of manufacturing errors on the friction and wear performance cannot be effectively revealed in this work.

3.3 Time-Domain Vibration Analysis

The time-domain vibration signals of different groups were collected in the X-axis/tangential and Y-axis/normal directions (see Figs. 6 and

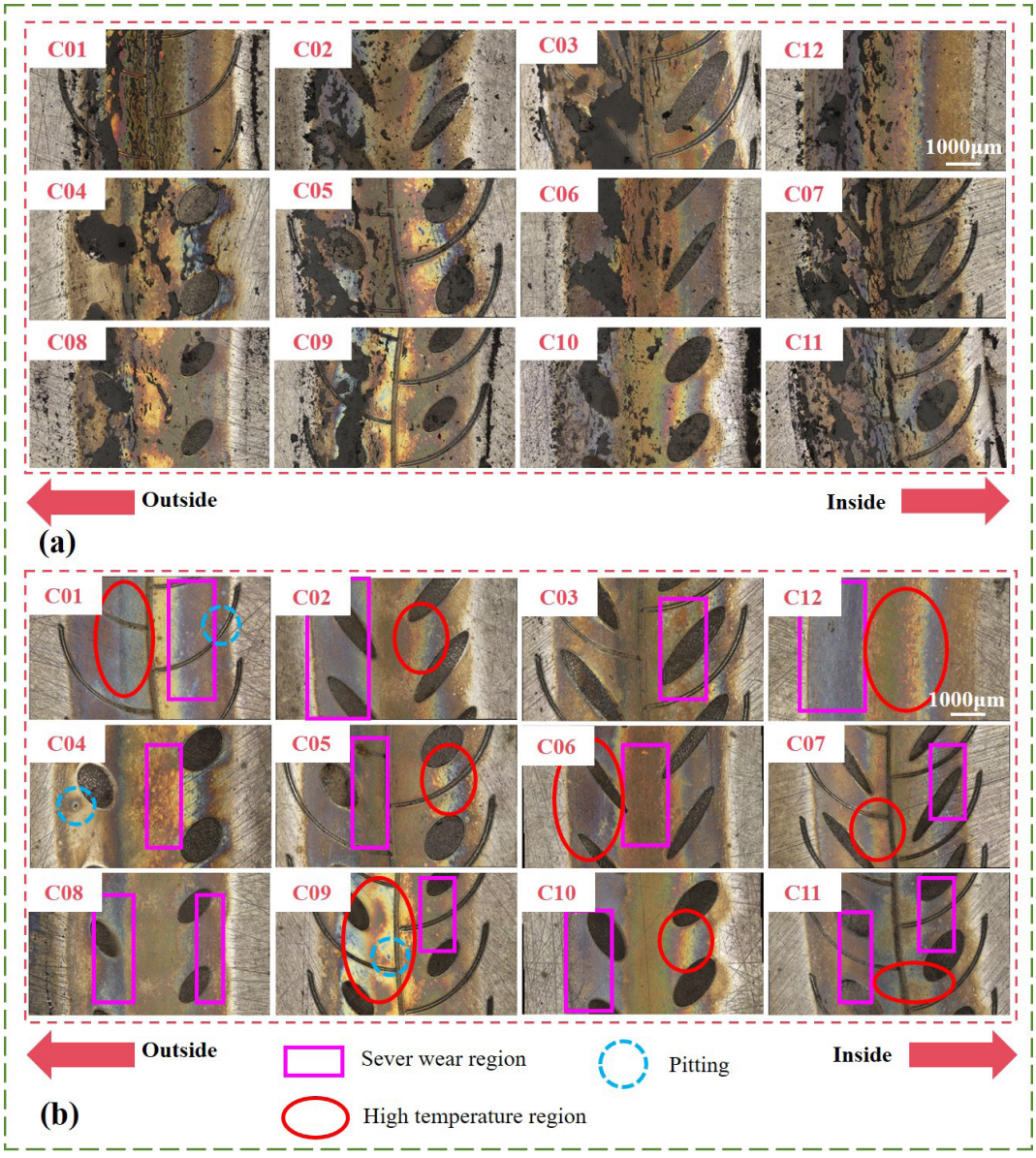

Fig. 5. Representative worn surfaces of the shaft washers of different groups; a) before ultrasonic washing, and b) after ultrasonic washing

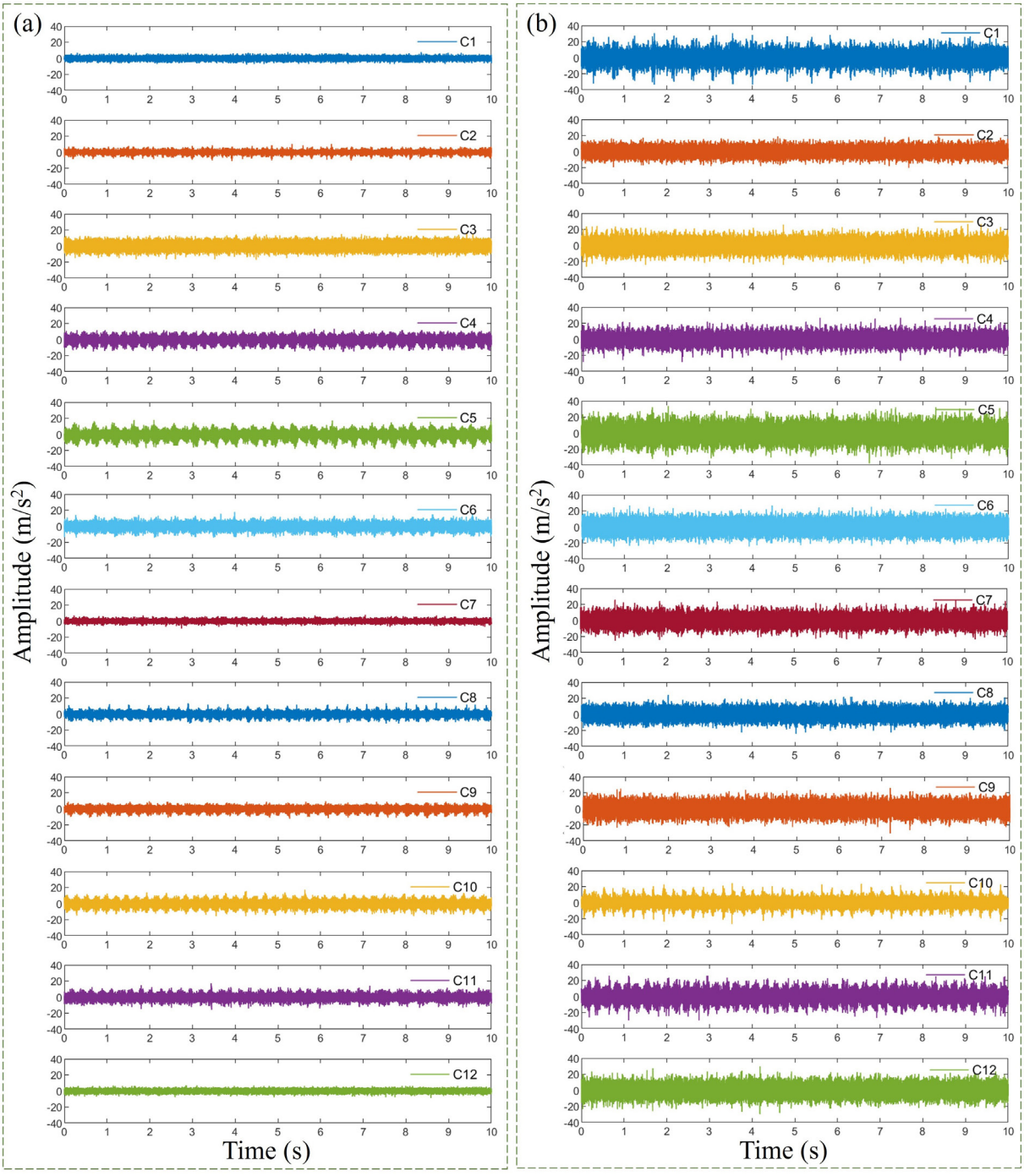

Fig. 6. Representative time-domain vibration signals of different groups from the 1800th s to the 1810th s;a) X-axis/Tangential direction, and b) Y-axis/Normal direction

7) to analyze the vibration characteristics in terms of peak values, root mean square (RMS), and crest factors (i.e., the ratio of peak value to RMS).

As shown in Fig. 6, during the early stages of the wear tests (i.e., from the 1800th s to the 1810th s), the time-domain signal amplitudes for both the smooth and the textured groups were much higher in the Y-axis/normal direction compared to the X-axis/tangential direction, due to the vertically applied load. The signal amplitudes of most biomimetic textured groups were larger than those of the smooth reference in both directions, with more periodic components. This was especially true for the groups with composite textures (elliptical holes combined with leaf veins, i.e., C03, C05, C07, C09, and C11), whose signal amplitudes were notably higher than the signals of those of the groups only with elliptical holes, i.e., C02, C04, C06, C08, and C10. This can be attributed to the fact that the textured surface changed the surface roughness and contact stiffness, thereby amplified the periodic vibration components [33].

As the tests neared their ends, i.e., from the 16,200th s to the 16,210th s (see Fig. 7), the time-domain signal amplitudes of all groups increased due to wear and the uneven distributed of the transfer film on the contact surfaces. Similarly, the signal amplitudes for both the smooth and the textured groups were much greater in the Y-axis/normal direction than in the X-axis/tangential direction. Therefore, the subsequent vibration analyses primarily focused on

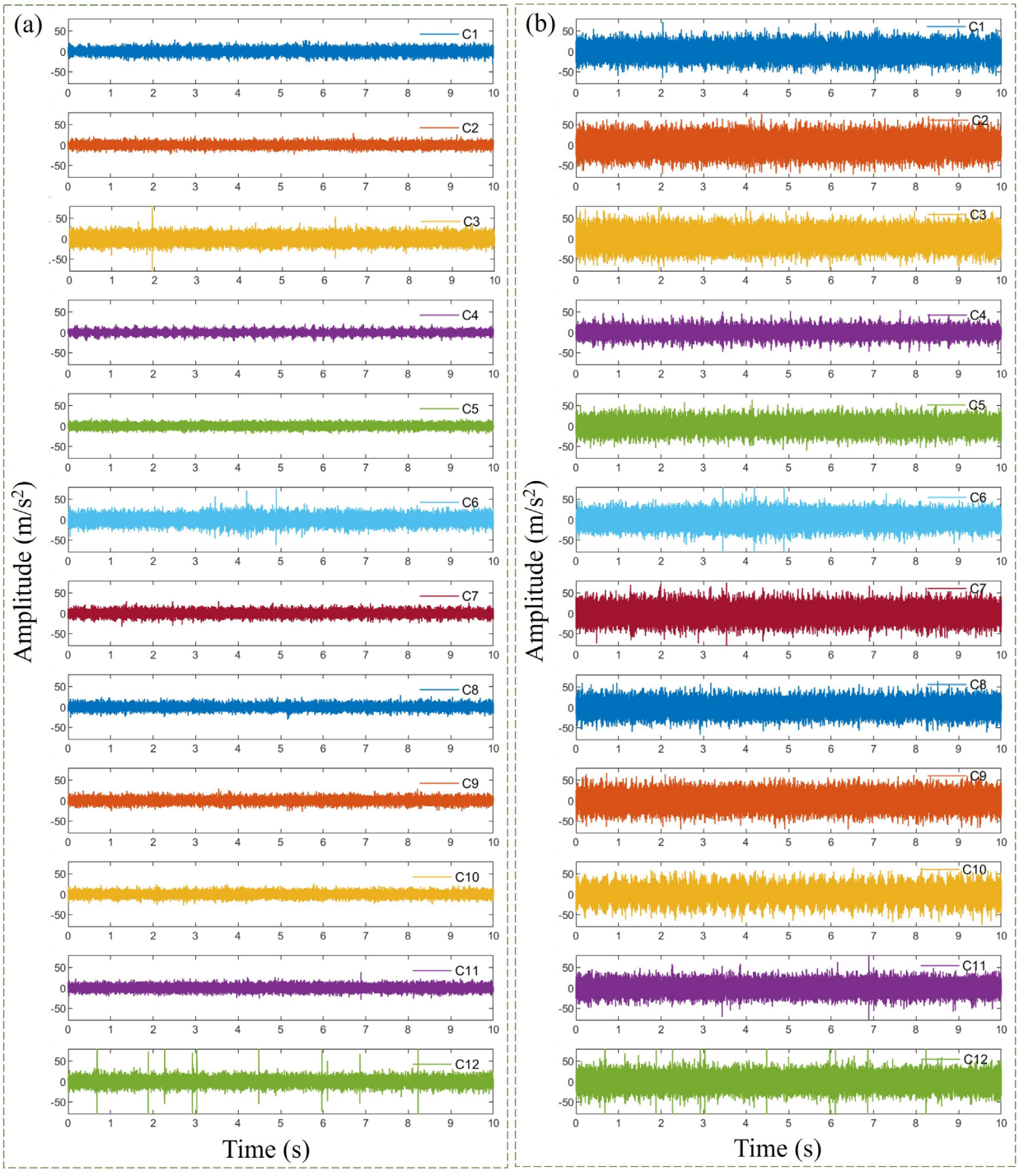

Fig. 7. Representative time-domain vibration signals of different groups from the 16200th s to the 16210th s; a) X-axis/ Tangential direction, and b) Y-axis/ Normal direction

the signals in the Y-axis direction [33]. Analyses of the signals in the X-axis direction can be found in the Supplementary Material. As shown in the figure, the signal amplitudes of the composite textured groups (i.e., C03, C05, C07, C09, and C11) were evidently higher than those of the groups with elliptical holes only (i.e., C02, C04, C06, C08, and C10). Due to the significant changes in surface roughness and contact stiffness of the textured surfaces, there were still many periodic components generated by the impact at the moment of contact that can be observed in their vibration signals. Among all twelve groups, the signal amplitude of C04 was the lowest in both directions.

Figure 8 shows the peak value, RMS and crest factor curves of different groups in the Y-axis/normal direction. As seen in the figure, the peak value, RMS and crest factor curves of the smooth group gradually increased and showed increasing trends in the later stage. Compared to the groups with elliptical holes only, the peak value and crest factor curves of C01, which had leaf veins only, were significantly higher, while its RMS curve was relatively lower. The presence of leaf-veins notably increased the time-domain characteristics of composite textured groups, i.e., C03, C05, C07, C09 and C11, particularly the peak value and RMS curves.

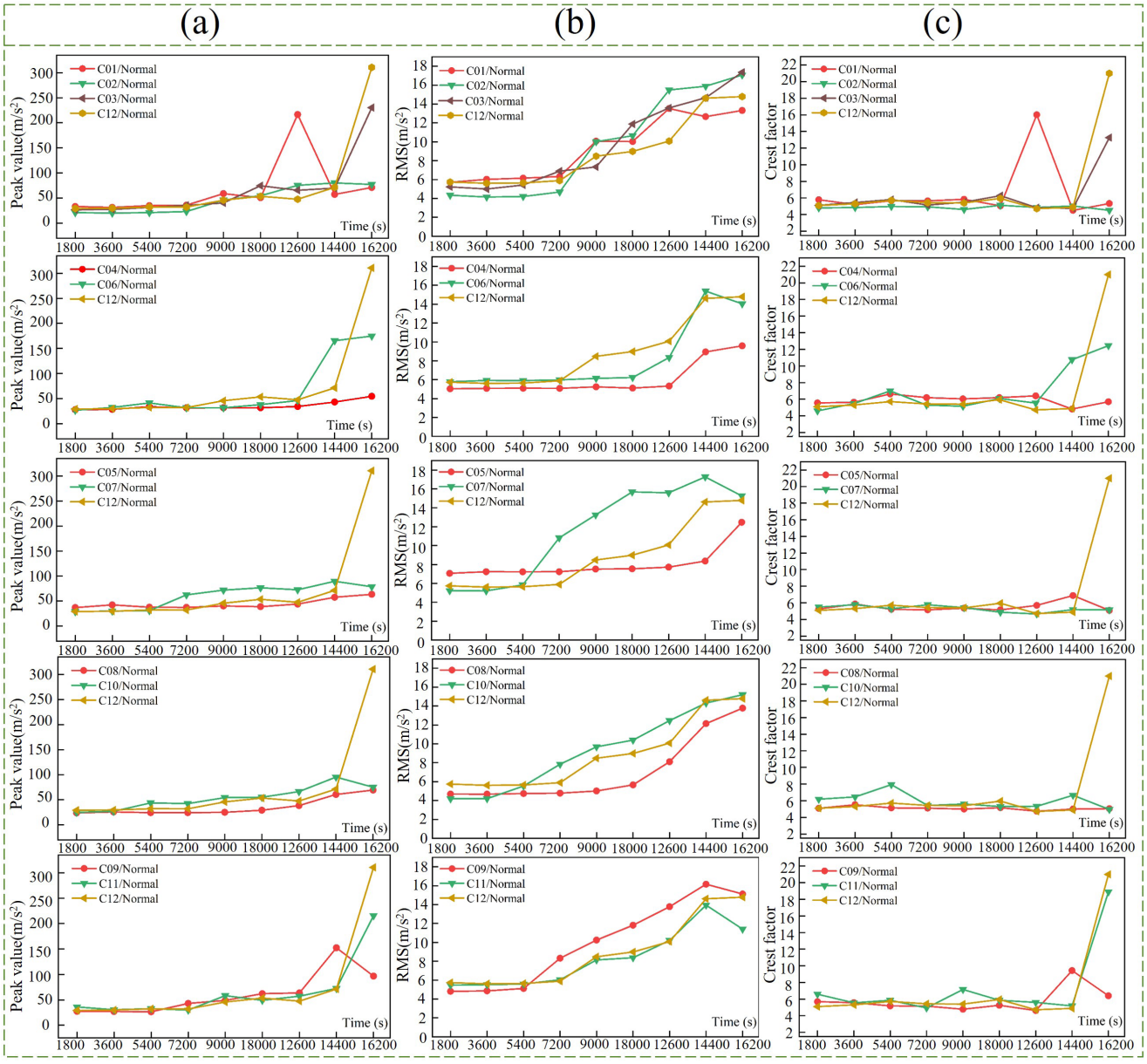

Fig. 8. Time-domain vibration characteristics curves in the Y-axis/normal directions; a) peak value curves, b) RMS curves, and c) crest factor curves

3.4 Frequency-Domain Vibration Analysis

Figure 9 shows the representative frequency-domain vibration signals in the Y-axis/normal direction for different groups at the 1,800th s and the 16,200th s, respectively. At the earlier time point, i.e., the 1,800th s, the frequency-domain vibration signals of C01, C02, and C03, as shown in Fig. 9a, indicated that leaf-veins significantly increased the frequency-peaks of the vibration signals in the range of 1000 Hz to 2000 Hz, while elliptical holes increased the frequency-peaks of the signals in the 0 Hz to 1000 Hz range, especially between 0 Hz to 300 Hz. The frequency-domain signal of C03 represented a coupling and superposition of the signals from C01 and C02. All groups exhibited notable frequency energy accumulation at around 1000 Hz and 1750 Hz. Biomimetic textured groups, in particular, had more periodic frequency-peaks in the low- frequency (LF) and mid-frequency (MF) ranges compared to the signals of the smooth reference [33]. The frequency-domain vibration signals of C04-C08 were generally lower than those of the other textured groups. At the 16,200th s, all groups showed more prominent and significant energy accumulation at 1000 Hz and 1750 Hz again. The signal amplitude of C04 was almost the lowest among all the biomimetic textured groups, followed by C11.

Figure 10 shows the representative power spectral density (PSD) curves of the frequency-domain vibration signals for different groups in the Y-axis/normal directions at the 1,800th s and the 16,200th s. As shown in Fig. 10a, the PSD curves of the leaf-geometry textured groups exhibited similar trends to those of the smooth group, making them difficult to distinguish as they overlapped at the 1800th s. However, compared to the PSD curve of the smooth group, the biomimetic textured groups showed more significant frequency-peaks in the LF-MF bands at this point [33]. By the 16,200th s, the frequency-peaks in the LF-MF bands for the biomimetic textured groups had either disappeared or been significantly reduced (see Fig. 10b). The PSD curves of these leaf-geometry textured groups were only slightly higher than that of smooth reference in the 1700 Hz to 2250 Hz range, and were lower in all other frequency ranges.

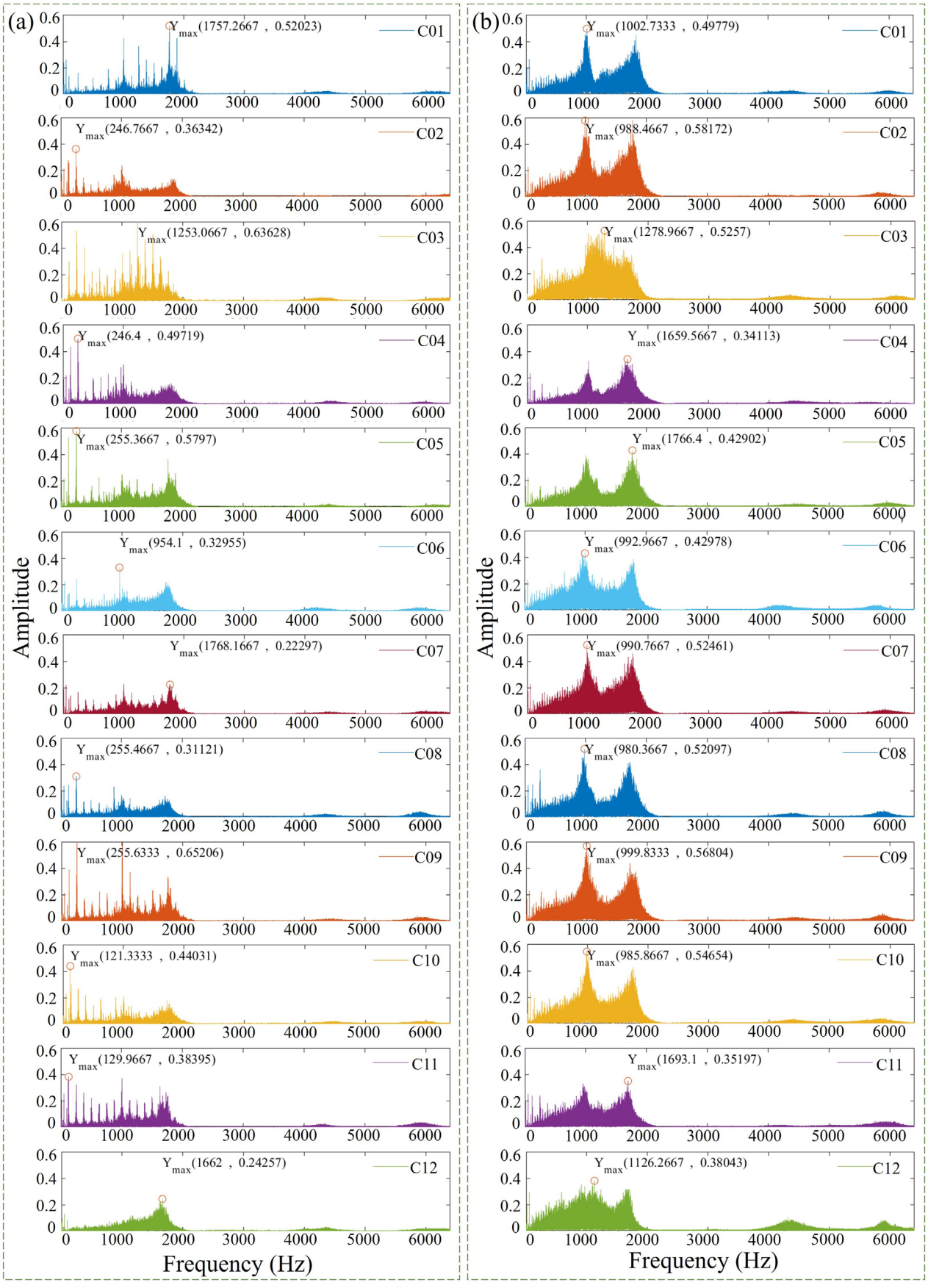

Fig. 9. Representative frequency-domain vibration signals for different groups in the Y-axis/normal direction at: (a) the 1800th s; (b) the 16200th s

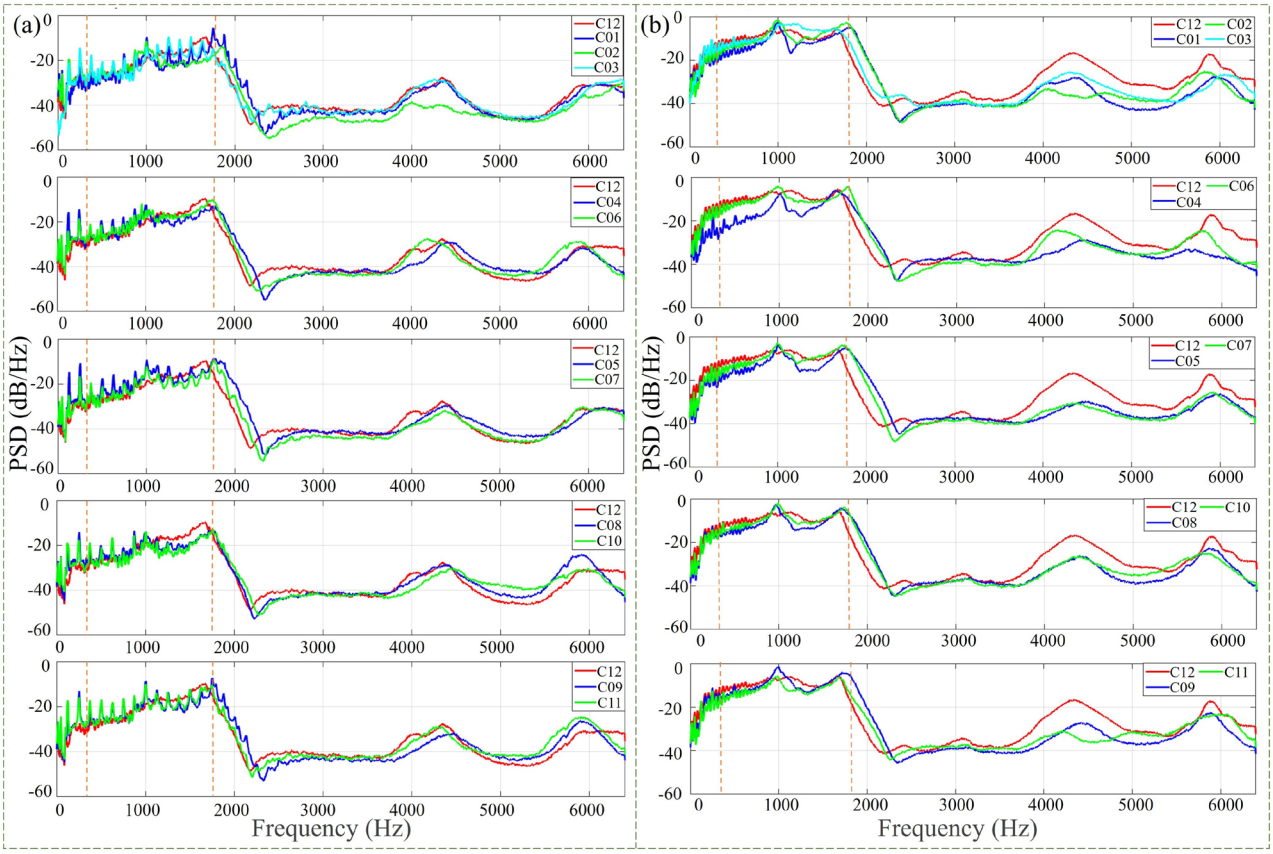

Fig. 10. PSD curves for different groups in the Y-axis/normal direction at; a) the 1800th s, and b) the 16200th s

4 DISCUSSIONS

Textures can tune the friction, wear, and vibration behavior of tribo-pairs through several mechanisms: collecting debris to reduce abrasive wear; "secondary lubrication" to improve the lubrication behavior under oil-starved lubrication; generating "Micro-eddies" to enhance the load- bearing capacity under elastohydrodynamic lubrication (EHL) or hydrodynamic lubrication (HL); varying contact stress to improve contact fatigue performance; and interrupting continuous thermal conduction to mitigate the "heat accumulation" phenomenon [3,33,35]. For the leaf-geometry biomimetic textures discussed in this article, the specific mechanisms were analyzed as discussed below.

4.1 Synergic Effect of the Elliptical Holes and Leaf Veins

Among the groups with elliptical holes only (i.e., C02, C04, C06, C08 and C10), C04 and C06 exhibited the longest mild-friction durations (11900 s and 12500 s, respectively), followed by C08 and C10. The mild-friction period of C10 lasted about 11500 s. The COF curves for C04, C06, and C08 failed to stabilize by the end of the tests and continued to fluctuate significantly (see Fig. 3). Since the average COF was calculated as the mean over the entire curve, this explains their lower average COFs in this work. The high average COF of C02 can be attributed to its largest texture area ratio among the five groups.

Regarding C01, the group with the vein-like textures only, its average COF was the highest among all the biomimetic textured groups (C01-C11), even surpassing that of the smooth reference. When coupled with the elliptical holes, leaf-veins significantly shortened the mild-friction durations of the composite textured groups, i.e., C03, C05, C07, C09 and C11. Consequently, their average COFs generally increased compared to the groups with elliptical holes only, except for C09. This can be attributed to the larger area ratios of the coupled leaf-geometry patterns, which reduced the effective contact area between the rollers and the raceways, naturally increasing the average COF [3,33]. However, composite textures also have the advantages of storing more lubricant and trapping more wear debris, which helps to reduce the frictional resistance of the bearings to some extent [36,37]. Ultimately, the friction-reducing performance was determined by the combined effects of those two opposing factors, along with the amount of the transfer film left on the raceways.

In terms of the wear amounts of the shaft washers, the group with vein-like textures only (C01) exhibited a higher wear loss (see Figs. 4a and 11a), significantly surpassing that of the smooth reference. Among the groups that only had elliptical holes (i.e., C02, C04, C06, C08, and C10), the wear losses of C02 and C04 were relatively low, while C06 and C08 experienced significantly higher wear, even exceeding that of C01. This can be attributed to the fact that leaf-geometry textures with a larger area ratio are more effective at trapping lubricant and capturing and retaining wear-debris, which helps to reduce wear of the contact surfaces (see Fig. 11b, d) [3,30,33].

When the elliptical holes coupled with the leaf-vein textures, the wear amounts of C03 and C05 increased compared to C02 and C04. In contrast, the wear losses of C07, C09, and C11 decreased significantly. This is because the wear losses of C02 and C04 were already quite low. The addition of the leaf-veins greatly increased the area ratios of the textured raceways (to 30.62 % and 24 %, respectively), thereby reducing surface rigidity and degrading the wear resistance of the "washers-rollers-cage" system. Due to their relatively small area ratios, the wear losses of C06 and C08 were

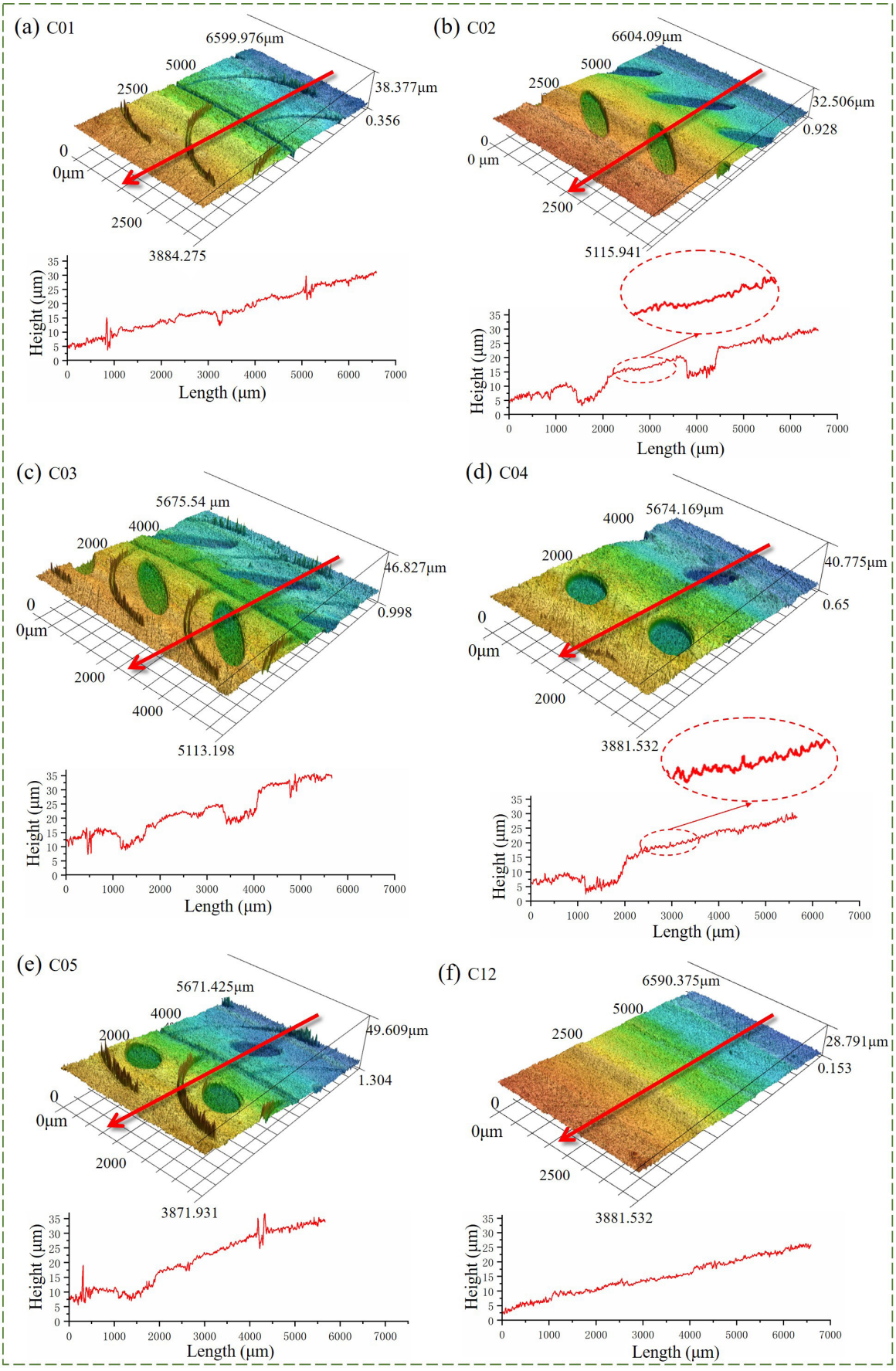

Fig. 11. Representative 3D morphologies and cross-sectional profiles of the worn surfaces for; a) C01, b) C02, c) C03, d) C04, e) C05, and f) C12

already high. After the addition of the leaf-vein textures, their area ratios further increased to 24 % and 20.69 %, respectively, resulting in a significant improvement in wear resistance instead. The wear amount of C10 was moderate, but after the leaf-vein textures were added, its area ratio rose to 28.41 %, leading to a significant reduction in wear loss.

The time-domain vibration signal of C01 initially exhibited strong periodic fluctuations, which subsided in the later stage [33]. Its peak value and crest factor curves rose significantly towards the end of the test. The groups only with elliptical holes showed lower time-domain signal amplitudes. The signal of C02 remained relatively smooth overall, with a relatively high RMS curve finally. When the elliptical holes were coupled with the leaf-vein textures, the amplitudes and periodic fluctuations of their signals generally increased throughout the whole tests, except for C11, which was consistent with their higher peak value and RMS curves. Both the signals of C04 and C10 showed pronounced fluctuations throughout the tests, due to the combined effects of their A/B ratios and elliptical areas. Compared to C10, C04 displayed significantly lower peak value and RMS curves.

The frequency-domain vibration signal of C01 exhibited many frequency peaks between 1000 Hz to 2000 Hz at the 1800th s. In contrast, elliptical holes primarily increased the amplitudes of the frequency peaks in 0 Hz to 1000 Hz range for the signals of C02, C04, C06, C08 and C10, which was consistent with their prominent peaks observed in their PSD curves in the LF-MF bands (see Fig. 10) [33,35]. The composite textured groups displayed numerous distinct frequency peaks in both the frequency-domain signals and PSD curves between 0 Hz to 1800 Hz at the 1800th s, leading to a significant "superposition effect", particularly in C03, C09, and C11 (see Fig. 9). The number of frequency peaks in C05 and C07 showed little change compared to C04 and C06. Their PSD curves remained largely consistent with smooth reference above 2400 Hz due to their area ratios.

At the 16,200th s, the coupling-induced "superposition effect" weakened but continued to amplify the maximum frequency peak of the bearings. The peaks of the PSD curves became nearly indiscernible above 1000 Hz. The frequency-domain vibration signals of C04-C07 increased slightly, with C04 and C05 showing significantly depressed PSD curves in their LF-MF bands compared to the smooth and other textured groups. These curves flattened beyond 2400 Hz and dropped markedly below those of the smooth group above 3500 Hz, particularly for C04. The PSD curves of C06 and C07 were lower in the LF-MF bands and showed a significant reduction beyond 3400 Hz. For C08-C11, the signals of the composite textured groups decreased but remained distinctly higher than those of C04-C07. Their PSD curves clustered similar to the smooth group in the LF-MF bands and were marginally lower beyond 3000 Hz, with few indistinguishable differences in certain frequency bands.

Therefore, the addition of leaf-veins increased the average COFs of the groups with elliptical holes only. The wear amount of each group was more closely related to its area ratio. When the leaf veins and elliptical holes were coupled, there was a significant "superposition effect" for the vibration signals in the earlier stages, amplifying the maximum frequency peak of the signals in the later stages.

4.2 Effect of the A/B Ratios and Areas of Elliptical Holes

4.2.1 Same Elliptical-Hole Area and Different A/B Ratios

For the biomimetic textured groups with the same elliptical-hole area, namely C04-C07, the average COFs of C04 and C06 were relatively lower due to their longer mild-friction durations. The wear losses of these four groups showed a significant increase in C06, rising from 5.75 mg (C04) to 8.31 mg. This can be attributed to the large A/B ratio of C06, which exacerbated the "edge crushing" phenomenon of the textures, generating more debris and leading to severe abrasive wear, even though the area ratios of C04 and C06 were the same. Therefore, a larger A/B ratio did not necessarily improve the friction-wear performance of the biomimetic textured groups. The coupling of the leaf-veins increased the average COFs of the composite textured groups (i.e., C05 and C07), but also significantly reduced the wear loss of C07. The high wear amount of C08 can be attributed to its small area ratio, which limited its ability to store lubricant and trap debris.

The time-domain vibration signal of C04 exhibited strong fluctuations, with its amplitude being the lowest among four groups throughout the entire test. In comparison to C04, the peak value, RMS, and crest factor curves of C06 were higher in the later stage. The peak value and RMS curves of C07 were also higher than those of C06, which was consistent with its larger average COF. Regarding the frequency-domain vibration signals, a larger A/B ratio helped reduce the amplitudes of the frequency peaks in the 0 Hz to 1000 Hz range at the 1,800th s, but did not contribute to reducing the signal amplitudes at the 16,200th s. The PSD curves of the four groups were largely similar at the 1,800th s, with C04 and C06 displaying larger frequency peaks. By the 16,200th s, when the A/B ratio was smaller, the PSD curves of C04 and C05 were significantly lower than both the smooth group and those of C06 and C07 in the LF-MF bands.

In general, a larger A/B ratio may deteriorate the friction-wear performance of the biomimetic textured groups. It reduced the amplitudes of the frequency peaks in the 0 Hz to 1000 Hz range during the earlier stages but increased the signal amplitudes in the later stages. When the A/B ratio was small, the groups tended to exhibit lower peak value, RMS, crest factor, and PSD curves. Overall, the tribological performance of C04 was superior. Its time-domain vibration signal showed strong fluctuations, but its amplitude was the lowest among all the biomimetic textured groups.

4.2.2 Same A/B Ratio and Different Elliptical-Hole Area

Regarding the biomimetic textured groups with the same A/B ratio (i.e., C08-C011), their mild-friction durations were quite long. The mild-friction duration of C11 was slightly shorter but still longer than that of the smooth reference, which explains why their average COFs were lower than that of smooth group. The COF curves of C08-C09 did not stabilize by the end of the tests and continue to rise. This answered why their average COFs were relatively high compared to C10. Meanwhile, the mass losses of C08-C11 decreased sequentially, with the wear losses of C09-C11 being lower than those of the smooth reference. Among these, the wear losses of C10 and C11 were lower than those of C08 and C09, with C11 exhibiting the lowest wear amount, only 4.91 mg.

The time-domain signal fluctuation of C10 was strong throughout the test, but its signal amplitude in the early stage was even the lowest among all groups. The peak value and RMS curves of C10 were significantly higher than those of C08 and the smooth reference. In contrast, the peak value and RMS curves of C08 were notably lower than those of the smooth group. The signal fluctuation of C11 was more pronounced in the early stage but became much more stable in the later stage with the smallest amplitude among the four groups. Its peak value and RMS curves were close to those of the smooth group, also lower than those of C09.

The frequency-domain vibration signals of the four groups were not significantly different at the 1800th s, and their PSD curves are generally similar, except in the 4400 Hz to 6100 Hz range. The frequency peaks of C08 and C10 were larger, with the PSD curve of C08 being slightly elevated. At the 16200th s, the difference between

the signals of the four groups remained minimal, and the signal amplitude of C11 was actually smaller. The PSD curves of the groups with smaller elliptical-hole areas (0.18π, i.e., C08 and C09) were almost identical. The PSD curves of C10 and C11 overlapped with those of C08 and C09, but with more pronounced differences.

So, when the elliptic-hole area was large, the wear losses of C10 and C11were 4.91 mg and 6.08 mg, respectively, both of which were lower than those of C08 and C09. Although their average COFs were relatively higher than those of C08 and C09, they were still lower than those of smooth group. The influences of elliptic-hole areas on the frequency-domain vibration signals of the four groups were not significant, and their PSD curves were generally similar, whether at the 1800th s or the 16200th s.

4.3 Influence Mechanism of the Leaf-Geometry Biomimetic Textures

As the rolling bearing rotates under oil-starved lubrication, the lubricant quickly flows away after being applied prior to test due to centrifugal force [38]. Without replenishment of lubricant afterwards, when the remaining lubricant on the raceway is insufficient to form a continuous and stable lubricating film, the bearing enters boundary lubrication (BL), followed by dry friction [35]. Correspondingly, nylon debris is generated from direct contact between the rollers and cage pockets and is transferred radially from the inside to the outside of the shaft washer under the influence of centrifugal force [3,30,38].

Under the combined effects of continuous rolling of rollers, friction-induced localized high temperature, and the overall temperature rise of the bearing, debris accumulates on the outer side of the raceway, forming discontinuous a nylon transfer film. Meanwhile, metal debris is also generated due to fatigue-spalling, which can create severe wear furrows on the raceway. As the bearing enters dry friction regime, the increased bearing temperature and local flash temperature lead to significant high-temperature ablation of the raceway. Due to the relatively large sliding-rolling velocities of the rollers near the outer edge of raceway, wear in this region becomes more severe (as seen in the worn-out costal veins and the unclear edges of the holes in Fig. 5b) [36,37].

Leaf-veins and elliptical holes enhance the lubrication of the "washers-rollers-cage" system through a "secondary lubrication effect" by storing more lubricant and trapping wear debris on the contact surface [3,30,33]. However, they also increase localized contact stresses, which can lead to material spalling and severe "edge crushing" phenomenon [33,36,37]. The influence of leaf-veins and elliptical holes on the tribological performance and friction-induced vibration behavior of bearings were analyzed from the following three perspectives:

1. Synergistic effect of leaf-veins and elliptical holes: In addition to the aforementioned effects, the main veins can also hinder the radial migration of wear debris, leading to its accumulation (see the black materials blocked in the main veins in Figs. 5a and 12a and b), ultimately exacerbating wear on the contact surfaces, especially when the costal veins are asymmetrically distributed. This explains the high wear and average COF observed in C01. However, asymmetric costal veins can also help slow down the rapid loss of lubricating oil, thereby extending the duration of

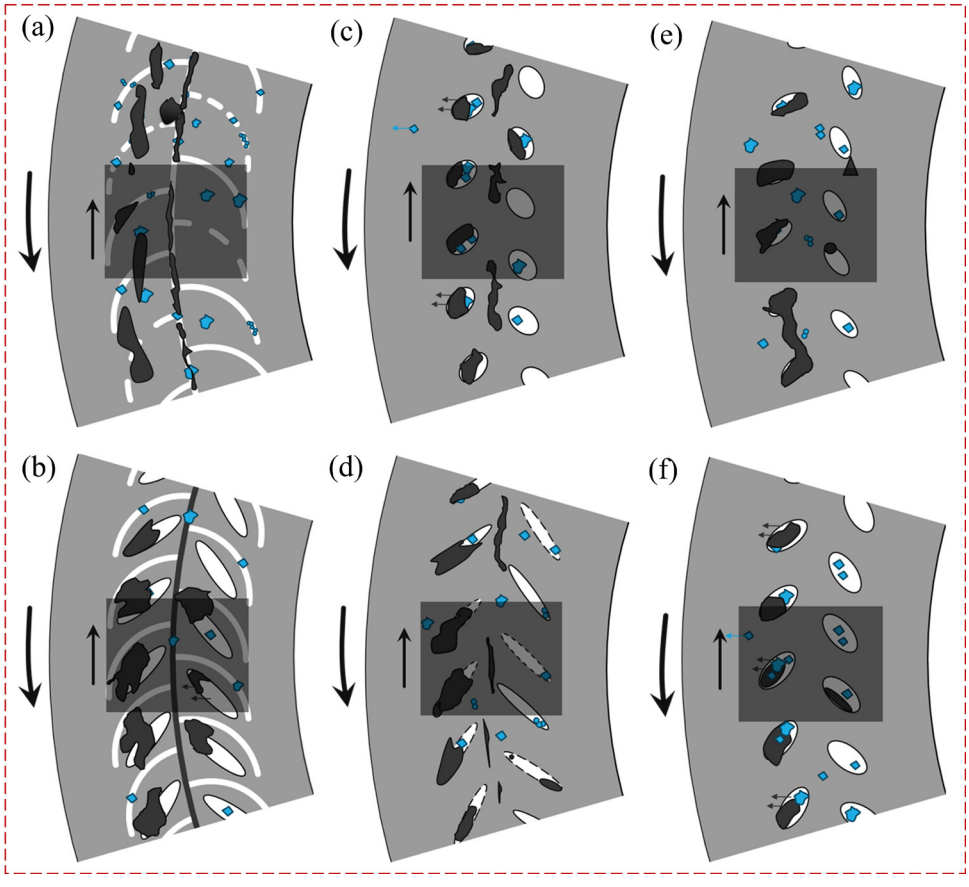

Fig. 12. Influence mechanism of leaf-geometry characteristics on the tribological performance of bearings: a,b) synergistic effect of leaf-veins and elliptical holes, c,d) influence of different A/B ratios, and e,f) influence of different elliptical area Note: black regions indicate the transfer film; blue arrows indicate the movement direction of wear debris; blue blocks indicate the wear debris.

the mild-friction stage. This is the reason why asymmetric costal veins were chosen in this work [3,33]. By the end of the tribo-test, little transfer film remained on the raceway, and the transfer film was unevenly concentrated between the outer costal veins and the main vein. This further contributes to the poor tribological and vibration performance of C01.

For the group only with elliptical holes, the absence of textures in the center of the raceway and the radially distributed costal veins means elliptical holes cannot effectively capture and store the migrating debris, resulting in more severe wear in the central zone and realizing a relatively longer "secondary lubrication" duration (see Figs. 3 and 11b and d). By the end of the tribo-test, the outer elliptical holes, filled with wear debris and repeatedly crushed by rollers, ultimately act as a "cushion" to improve the vibration performance of the bearing [33].

When leaf-veins coupled with elliptical holes, the area ratio of the textured surface increases significantly, allowing for more lubricating oil to be stored in the initial stage. This promotes better "secondary lubrication" [39]. However, the presence of costal veins also accelerates the loss of lubricating oil, so the final secondary lubrication time is comparable to, or only slightly longer than, that of the group with leaf-veins only. The synergistic effect of leaf veins and elliptical holes also results in a denser and more patchy distribution of the transfer film between the costal veins and the main vein on the outer side of the raceway (see C03 in Fig. 5a). This may be due to the interaction between the leaf veins and elliptical holes during the radial migration of debris, which leads to stronger vibration signals and more periodic components compared to the groups with elliptical holes only. As a result, only slight wear marks were observed on the raceways of the shaft washers of these composite textured groups, with no noticeable deep scratches.

2. Influence of different A/B ratios of elliptical holes with the same area: When the elliptical -hole area is the same, a larger A/B ratio results in a larger circumference of the elliptical hole ($L=2\pi B+4(A-B)$, see Table 2), longer coverage length in the radial direction, and sharp corners in the long axis direction. These factors contribute to enhanced "secondary lubrication" in the "washers- rollers-cage" system, thereby extending the mild-friction duration of the bearing. However, the longer radial coverage length and flat morphology also facilitate debris accumulation at the ends of the long axis. This, in turn, exacerbates fluctuation in frictional resistance and leads to severe wear on the raceway during boundary lubrication and dry friction stages, ultimately deteriorating the vibration performance of the bearing. Additionally, the coupling of leaf veins influences the radial migration of debris, causing the residual transfer film to become more uneven. This increases the bearing's frictional resistance and further degrades its vibration behavior.
3. Influence of different areas of elliptical holes with the same A/B ratio: When the A/B ratio is fixed, a large elliptical area means a larger elliptical hole, which can store more lubricating oil, achieve a better "secondary lubrication" effect, and extend the duration of mild-friction stage of the bearing (see Fig. 3c). This also allows for the trapping and storing more debris, which reduces the residual transfer film and wear debris on the contact surface, thereby improving the wear resistance of the bearing (see Fig. 4a), and lowering the increase in friction resistance during the boundary lubrication and dry friction stages. Due to the unchanged shape, the impact of different elliptical hole areas on the time-domain and frequency-domain vibration signals is not significant. Nonetheless, larger elliptical holes can still slightly reduce the stiffness of the contact surface and increase the frequency-peak values of the vibration signals.

5 CONCLUSIONS

Inspired by the unique leaves of *Monstera deliciosa*, various leaf-geometry patterns were designed and prepared on the shaft washers of 81107TN bearings. The effects of leaf-veins and elliptical holes (with different A/B ratios and elliptical areas) on the tribological performance and friction-induced vibration behavior of rolling bearings were investigated under starved lubrication. Based on the data obtained, the following conclusions can be drawn:

1. The group with only leaf-veins exhibited the highest average COF among all twelve groups, along with relatively large wear loss. Its time-domain vibration signals showed strong periodic fluctuation initially, which subsided in the later stage. The peak value and crest factor curves remained relatively high towards the end of the test. In the frequency-domain, its vibration signals demonstrated many frequency peaks between 1000 Hz to 2000 Hz during the earlier stage. Groups with elliptical holes only (i.e., C02, C04, C06, C08 and C10) demonstrated relatively smaller average COFs, lower time-domain vibration signals and an increase in the amplitudes of the frequency peaks predominantly in the 0 Hz to 1000 Hz range. When leaf veins were coupled with elliptical holes, the average COFs of bearings increased. This also generated a significant "superposition effect" in the time-domain vibration signals during the earlier stages and amplified the maximum frequency peak in the frequency-domain vibration signals during the later periods.
2. When the A/B ratio was larger, i.e., 6.0, the friction-wear performance of the biomimetic textured groups deteriorated. In contrast, when the A/B ratio was small (1.5, as in C04 and C05), the groups tended to have relatively low peak value, RMS, crest factor, and PSD curves.
3. When the elliptic area was large (0.32π mm2), the average COFs of C10 and C11 were relatively higher than those of C08 and C09, whose elliptic area was only 0.18π mm2. The wear losses of C10 and C11 were 4.91 mg and 6.08 mg, respectively, both lower than those of C08 and C09. The influence of different elliptic areas on frequency-domain vibration signals of the four groups was not obvious.
4. Among the twelve groups, C04 exhibited the best overall tribological and friction-induced vibration performance. Compared to the smooth reference, its average COF was reduced by 13 % and its wear amount decreased by 5.3 %. Its time-domain and frequency-domain vibration signals were the lowest, or relatively low, among all the groups and noticeably lower than those of the smooth reference.

Finally, this paper only explored the impact of leaf-geometric characteristics on the tribological and friction-induced vibration performance of rolling bearings. Research on the significance and optimization of various influencing factors is ongoing, and the relevant results will be shared in the future.

References

[1] Holmberg, K., Erdemir, A. Influence of tribology on global energy consumption, costs and emissions. *Friction* 5 263-284 (2017) **DOI:10.1007/s40544-017-0183-5**.

[2] Holmberg, K., Erdemir, A. The impact of tribology on energy use and CO2 emission globally and in combustion engine and electric cars. *Tribol Int* 135 389-396 (2019) **DOI:10.1016/j.triboint.2019.03.024**.

[3] Zhao, C., Long, R.S., Zhang, Y.M., Wang, Y.B., Wang, Y.Y. Influence of characteristic parameters on the tribological properties of vein-bionic textured

cylindrical roller thrust bearings. *Tribol Int* 175 107861 (2022) **DOI:10.1016/j.triboint.2022.107861**.

[4] Gachot, C., Rosenkranz, A., Hsu, S.M., Costa, H.L. A critical assessment of surface texturing for friction and wear improvement. *Wear* 372 21-41 (2017) **DOI:10.1016/j.wear.2016.11.020**.

[5] Zhang Q.C., Li Y., Liang F., Zhang H.R., Wang B., Li X.P., et al. Tailoring tribological characteristics in titanium alloys by laser surface texturing and 2D Ti3C2Tx MXene nanocoating. *Adv Funct Mater* 34 2401231 (2024) **DOI:10.1002/adfm.202401231**.

[6] MacLucas T., Grützmacher P.G., Leonhard-Trautmann P., Suarez S., Gachot C., Mücklich F. Combining carbon nanoparticle coatings and laser surface texturing for enhanced lubricity under high loads. Tribol Letter 72 38 (2024) **DOI:10.1007/s11249-024-01837-5**.

[7] Xu, X., Zhang, Y.M. Effect of different chemical conversion coatings on the tribological performance of cylindrical thrust roller bearings under conditions of dry friction and solid lubrication. *Wear* 548 205351 (2024) **DOI:10.1016/j.wear.2024.205351**.

[8] Liu, J., Li, X.B. A review of calculation and analysis methods of friction torques and power losses of rolling element bearings. *Mech Based Des Struct Mach* 53 7783-7803 (2025) **DOI:10.1080/15397734.2025.2500661**.

[9] Liu, J.Y., Li, X.B., Xu, Y.J., Zhang, Y., An, Y.C. Liu J. Analysis of contact characteristics in an innovative DGBB with a multi-hollow outer ring. *Chin J Mech Eng* (2026) In Press **DOI:10.1016/j.cjme.2025.100211**.

[10] Grützmacher, P.G., Rosenkranz, A., Szurdak, A., Grüber, M., Gachot, C., Hirt, G., et al. Multi-scale surface patterning-an approach to control friction and lubricant migration in lubricated systems. *Ind Lubr Tribol* 71 1007-1016 (2019) **DOI:10.1108/ILT-07-2018-0273**.

[11] Ma, J., Liu, Y.C., Yi, P., Jia, H.Y., Zhang, N., Sun, J.W. Anti-friction mechanism of sinusoidal texture with various intervals: The synergistic effect of dynamic pressure and tribofilm. *Tribol Int* 173 107635 (2022) **DOI:10.1016/j.triboint.2022.107635**.

[12] Rosenkranz, A., Costa, H.L., Baykara, M.Z., Martini, A. Synergetic effects of surface texturing and solid lubricants to tailor friction and wear - A review. *Tribol Int* 155 106792 (2021) **DOI:10.1016/j.triboint.2020.106792**.

[13] Liu, W.L., Ni, H.J., Chen, H.L., Wang, P. Numerical simulation and experimental investigation on tribological performance of micro-dimples textured surface under hydrodynamic lubrication. *Int J Mech Sci* 163 105095 (2019) **DOI:10.1016/j.ijmecsci.2019.105095**.

[14] Gropper, D., Wang, L., Harvey, T.J. Hydrodynamic lubrication of textured surfaces: A review of modeling techniques and key findings. *Tribol Int* 94 509-529 (2016) **DOI:10.1016/j.triboint.2015.10.009**.

[15] Rosenkranz, A., Grützmacher, P.G., Gachot, C., Costa, H.L. Surface texturing in machine elements– a critical discussion for rolling and sliding contacts. *Adv Eng Mater* 21 1900194 (2019) **DOI:10.1002/adem.201900194**.

[16] Feringa, F., Bauer, G.E.W., Van Wees, B.J. Observation of magnetization surface textures of the van der Waals antiferromagnet FePS3 by spin Hall magnetoresistance. *Phys Rev B* 105 214408 (2022) **DOI:10.1103/PhysRevB.105.214408**.

[17] Liem, N.V., Zhenpeng, W., Renqiang, J. Effect of shape/size and distribution of microgeometries of textures on tribo-performance of crankpin bearing. *Proc Inst Mech Eng J* 236 421-433 (2022) **DOI 10.1177/13506501211010552**.

[18] Guo, D., Zhang, P., Jiang, Y.Y., Song, C.F., Tan, D.Q., Yu, D.P. Effects of surface texturing and laminar plasma jet surface hardening on the tribological behaviors of GCr15 bearing steel. *Tribol Int* 169 107465 (2022) **DOI:10.1016/j.triboint.2022.107465**.

[19] Li, Y.W., Yang, H.W., Wiercigroch, M., Han, Y.F., Sun, S.L., Li, D.C., et al. Bionic structure inspired by tree frogs to enhance damping performance. *ACS Appl Mater Interfaces* 15 31979-31993 (2023) **DOI:10.1021/acsami.3c05095**.

[20] Wang, H.J., Qiu, H.A., Liu, W., Tian, L.L., Zheng, J., Zhang, Z.H. et al. Anti-wear properties of multi-bioinspired textures with hierarchical and superhydrophobic structures under water lubrication *Wear* 532 205124 (2023) **DOI:10.1016/j.wear.2023.205124**.

[21] Liu, Y., Zhang, H., Dai, S.J., Dong, G.N. Designing a bioinspired scaly textured surface for improving the tribological behaviors of starved lubrication. *Tribol Int* 173 107594 (2022) **DOI:10.1016/j.triboint.2022.107594**.

[22] Qin, L.G., Huang, X.D., Sun, Z.S., Ma, Z.Y., Mawignon, F.J., Lv, B.H., et al. Synergistic effect of sharkskin-inspired morphologies and surface chemistry on regulating stick-slip friction. *Tribol Int* 187 108765 (2023) **DOI:10.1016/j.triboint.2023.108765**.

[23] Li, Y.W., Yang, H.W., Wiercigroch, M., Han, Y.F., Sun, S.L., Li, D.C., et al. Bionic structure inspired by tree frogs to enhance damping performance. *ACS Appl Mater Interfaces* 15 31979-31993 (2023) **DOI:10.1021/acsami.3c05095**.

[24] Wang, H.H., Lin, N.M., Yuan, S., Liu, Z.Q., Yu, Y., Zeng, Q.F., et al. Numerical simulation on hydrodynamic lubrication performance of bionic multi-scale composite textures inspired by surface patterns of subcrenata and clam shells. *Tribol Int* 181 108335 (2023) **DOI:10.1016/j.triboint.2023.108335**.

[25] Khatri, C.B., Yadav, S.K., Thakre, G.D., Rajput, A.K. Design optimization of vein-bionic textured hydrodynamic journal bearing using genetic algorithm. *Acta Mech* 235 167-190 (2024) **DOI:10.1007/s00707-023-03734-9**.

[26] Zhang, Z.Q., Li, J.Y., Zou, T.G., Hou, W., An, Y.Y., Liu, J.H. Effect of bionic texture on the lubrication efficiency and mechanical efficiency loss for rotating gears. *Surf Topogr Metrol Prop* 12 035004 (2024) **DOI:10.1088/2051-672X/ad557b**.

[27] Song, F., Yang, X.F., Cong, J.C, Sun, J., Shao, S.B., Dong, W.L., et al. Tribological properties of YT15 alloy steel surfaces with different bionic textures. *J Mater Eng Perform* 33 586-600 (2024) **DOI:10.1007/s11665-023-08010-4**.

[28] Liang, Y.N., Zhang, F.C., Xing, H., Wang, C.Y., Chen, N., Wang, W., et al. Lubrication and wear characteristics of bionic composite texture on friction pair under seawater condition. *Surf Topogr Metrol Prop* 13 015023 (2025) **DOI:10.1088/2051-672X/adaed7**.

[29] Liu, W.Y., Hou, W.F., Ou, Y.X. Relationship between medial axis pattern of plant leaf and mechanics self-adaptability (I): Experimental investigation and numerical simulation. *J South China Univ Technol (Nat Sci Ed)* 35 42-46 (2007). (in Chinese)

[30] Long, R.S., Zhao, C., Zhang, Y.M., Wang, Y.B., Wang, Y.Y. Effect of vein-bionic surface textures on the tribological behavior of cylindrical roller thrust bearing under starved lubrication. *Sci Rep* 11 21238 (2021) **DOI:10.1038/s41598-021-00800-x**.

[31] Madison, M. A revision of Monstera (Araceae). *Contrib Gray Herb Harvard Univ* 207 3-100 (1977) **DOI:10.5962/p.336443**.

[32] Muir, C.D. How did the Swiss cheese plant get its holes? *Am Nat* 181 273-281 (2013) **DOI:10.1086/668819**.

[33] Long, R.S., Shang, Q.Y., Sun, S.N., Wang, S.W., Ma, C., Zhang, J.W., et al. Influence of Monstera riedrichsthalii bionic textures on the tribological and vibration behavior of rolling bearings. *Friction* 13 9440949 (2024) **DOI:10.26599/FRICT.2025.9440949**.

[34] Xiao, Q.H., Wang, X.Y., Wang, Y.Y., Zheng, W., Xu, J.W., Luo, X.C., et al. Beyond smoothness: the art of surface texturing battling against friction. *Int J Extrem Manuf* 7 022014 (2024) **DOI:10.1088/2631-7990/ad9c01**.

[35] Long, R.S., Sun, Y.H., Zhang, Y.M., Shang, Q.Y., Ramteke, S.M., Marian, M. Influence of micro-texture radial depth variations on the tribological and vibration characteristics of rolling bearings under starved lubrication. *Tribol Int* 194 109545 (2024) **DOI:10.1016/j.triboint.2024.109545**.

[36] Long, R.S., Li, M.H., Jin, Z.H., Zhang, Y.M., Han, H. Tribological behavior of pits textured multi-rollers sliding-rolling tribo-pair under periodic varied load and dry wear. *Adv Mech Eng* 14 (2022) 16878132221092520, **DOI:10.1177/16878132221092520**.

[37] Long, R.S., Pan, Z., Jin, Z.H., Zhang, Y.M, Sun, S.N, Wang, Y.Y., Tribological behavior of grooves textured thrust cylindrical roller bearings under dry wear. *Adv Mech Eng* 13 16878140211067284 (2021) **DOI:10.1177/16878140211067284**.

[38] Grützmacher, P.G., Rosenkranz, A., Rammacher, S., Gachot, C., Mücklich, F. The influence of centrifugal forces on friction and wear in rotational sliding. *Tribol Int* 116 256-263 (2017) **DOI:10.1016/j.triboint.2017.07.021**.

[39] Long, R.S., Yao, Y., Wang, H.M., Gao, F.F., Zong, L., Marian, M. Nature's blueprints on bearings: Tribological and vibration performance of leaf-shaped textures for thrust roller bearings under starved lubrication. *J Mater Res Technol* 39 9143-9158 (2025) **DOI:10.1016/j.jmrt.2025.11.185**.

[40] Long, R. Supplementary Material to "Leaf-geometry Characteristics of Monstera deliciosa: their Effects on the Tribological and Friction-induced Vibration Behavior of Rolling Bearings under Starved Lubrication". *Sci Data Bank* (2026) **DOI:10.57760/sciencedb.32618**.

Acknowledgements *R. Long greatly acknowledges the financial support from the Natural Science Foundation of Liaoning Province, China (No. 2023-MS-234), the Scientific Research Fund of Liaoning Provincial Education Department, China (No. LJ212510149017), the National Natural Science Foundation of China (No. 52275156), the National Natural Science Foundation of China Young Scientist Fund (No. 52402484) and the University-level doctoral special research start-up fund support project (Shenyang Polytechnic College, China, No.szy2024bs002).*

Received *2025-12-11,* **revised** *2026-04-06,* **accepted** *2026-04-16 as Original Scientific Paper.*

Author contributions *R. Long: Conceptualization, Investigation, Formal analysis, Writing – original draft; J. Chen: Conceptualization, Methodology, Investigation, Software; F. Gao: Conceptualization, Investigation; R. Huang: Conceptualization, Investigation; S. Gao: Conceptualization, Supervision; L. Zong: Conceptualization, Formal analysis, Writing – review & editing. All authors have reviewed, edited and read the final version.*

Data availability *The original data used to support the findings of this study are available from the corresponding author upon request.*

Supplementary Information *Supplementary Information provides essential descriptions and figures, that are critical to understanding the paper's content* **[40]**.

Geometrijske značilnosti listov Monstera deliciosa: vpliv na tribološko obnašanje in vibracije, povzročene s trenjem, pri kotalnih ležajih ob pomanjkljivem mazanju

Povzetek *Za podaljšanje življenjske dobe kotalnih ležajev in izboljšanje zanesljivosti pripadajočih mehanskih sistemov je bilo po navdihu listov rastline Monstera deliciosa zasnovanih enajst biomimetičnih teksturnih vzorcev. Ti vključujejo različne geometrijske značilnosti listov, kot so listne žile, eliptične odprtine in njihove kombinacije, ki so bile z lasersko teksturiranjem površine izdelane na tekalni stezi podložke valjčnih aksialnih ležajev. Vpliv teh vzorcev, navdihnjenih z listi, na tribološke lastnosti in vibracije, povzročene s trenjem, je bil sistematično preučen v pogojih pomanjkljivega mazanja. Rezultati kažejo, da je bil v začetnih fazah preizkušanja opažen izrazit »učinek superpozicije« v vibracijskih signalih, ki pa se je s časom zmanjšal. Večja razmerja stranic eliptičnih odprtin niso izboljšala triboloških lastnosti biomimetičnih tekstur. Pri večjih eliptičnih površinah so ležaji izkazovali manjšo obrabo, vendar višje povprečne koeficiente trenja in večja nihanja vibracijskih signalov v časovni domeni. Vpliv različnih velikosti eliptičnih površin na vibracijske signale v frekvenčni domeni je bil majhen. Raziskava ponuja pomembne vpoglede za optimizacijo tekalnih površin kotalnih ležajev.*

Ključne besede *kotalni ležaji, biomimetična površinska tekstura, tribologija in vibracije zaradi trenja, pomanjkljivo mazanje*